Journal of Advanced Zoology
ISSN: 0253-7214
Volume 44 Issue -05Year 2023 Page 492:507

Revolutionizing Agriculture With Nanotechnology: Rice-Based Silica Nanoparticles For The Remediation And Quantification Of Toxic Heavy Metals In Potatoes

Meetkumar Thakar[1a], Dave Gaurav S.[2b], Joshi Nirav D.[3c], Pankaj Sharma[a]*

[a*]*Department of Applied Chemistry, Faculty of Technology and Engineering, The Maharaja Sayajirao University of Baroda, Vadodara – 390 001, Gujarat, India*
[b]*Bio Science Research Centre, Sardarkrushinagar Dantiwada Agricultural University, Dantiwada-385505, Gujarat, India.*
[c]*College of Food Technology, Sardarkrushinagar Dantiwada Agricultural University, Dantiwada-385505, Gujarat, India*

***Corresponding Author:** Pankaj Sharma*
E mail: pankajrajsharma@gmail.com

Article History

Received:
Revised:
Accepted:

Abstract

Today, metal pollution in agricultural soils poses a growing concern due to its potential health risks through the consumption of contaminated plants like potatoes. Heavy metal concentrations in the environment can exceed safe levels due to various human activities, including industrialization, mining, and agricultural practices. Consequently, potatoes and other vegetables may contain toxic heavy metals like Co, Ni, Pb, Cd, and Cr. Effective removal techniques are needed to mitigate these risks to food safety and human health. In this study, a simple and inexpensive green synthesis method is described to extract mesoporous silica nanoparticles taken from Navsari region "GNR-3 (Gujarat Navsari Rice – 3)" rice using the bottom-up approach for removal of toxic heavy metals contamination present in North Gujarat region Banaskantha district's special variety potatoes named "KUFRI BADASHAH". Rice husk (RH) calcinated to obtain rice husk ash (RHA) with high silica purity (>98% wt), as determined by the EDX analysis. Calcination at 650°C for four hours in a box furnace yielded RHA that was devoid of metal impurities and organic matter. The present study defines successfully minimization of toxic heavy metal contamination present in potatoes by employing silica nanoparticles (SNPs) as a biomass adsorbent and also includes all basic characterization of SNPs. The X-ray diffraction pattern showed a broad peak at 2θ≈22.1°C and was free from any other sharp peaks, indicating the amorphous property of the GNR-3 variety rice SNPs. Scanning electron micrographs (SEM) showed clusters of spherically shaped uniform aggregates of SNPs while transmission electron microscopy analysis indicated an average particle size of < 50 nm. Peaks in the Fourier transform infrared spectra were found at 1083.29 cm^{-1} and 795.48 cm^{-1}, corresponding to O-Si-O symmetric stretching vibration and O-Si-O asymmetric stretching, respectively. The Brunauer-Emmet-Teller, obtained value of 11.1984 m^2/g reflects the extent of surface available for adsorption. Concurrently, the pore size, a crucial factor influencing the accessibility of adsorption sites, was

measured at 196.202 Å. The specific surface area of 11.1984 m^2/g suggests a considerable active surface for potential interactions, respectively. In conclusion, Agriculture waste-derived SNPs (Silver Nanoparticles) offer a compelling solution for the removal of toxic heavy metals from potatoes. This technique is characterized by its simplicity, as it leverages readily available agricultural waste materials, requiring minimal processing.

Keywords: Toxic heavy metals, potatoes, silica nanoparticles, rice husk ash, characterization of SiO_2, food product remediation.

Graphical Abstract

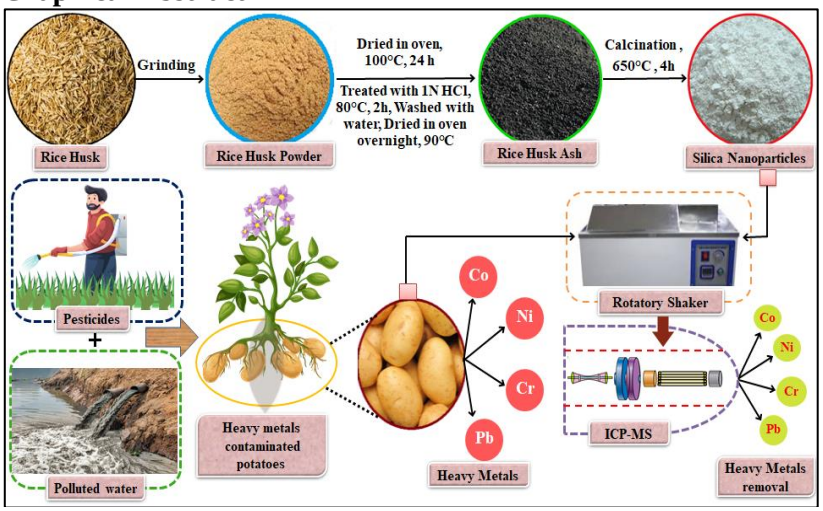

1. Introduction:

Toxic heavy metals in food products are a growing concern due to their potential health risks to Humans. Heavy metal contamination in potatoes, a staple food crop, can adversely affect human health. The quantification and remediation of heavy metals in potatoes are crucial for ensuring food safety and protecting public health [1]. This research paper focuses on the quantification of toxic heavy metals present in potatoes from the North Gujarat region "KFRI BADSHAH" and explores the use of silica nanoparticles synthesized from GNR-3 rice SNPs as a biomass adsorbent for food product remediation. Heavy metals, including Cobalt (Co), Nickel (Ni), lead (Pb), cadmium (Cd), and chromium (Cr), can enter the food chain through various sources such as soil, water, and agricultural inputs [2].

Accumulation of heavy metals in crops, particularly potatoes, can occur due to their uptake from contaminated soil or water during growth. Continuous consumption of heavy metal-contaminated potatoes can lead to chronic health issues, including organ damage, neurological disorders, and even cancer [3]. Therefore, it is crucial to monitor and quantify heavy metal concentrations in potatoes to assess potential health risks to consumers.

In this study, we employed an analytical technique called inductively coupled plasma mass spectrometry (ICP-MS) to quantify the concentrations of heavy metals in potato samples. ICP-MS is a highly sensitive and accurate method for determining trace elements, allowing for the precise measurement of heavy metal content in food samples [4].

To address the issue of heavy metal contamination in potatoes, we explored the use of SNPs synthesized from rice husk ash (RHA) as a potential remediation strategy. RHA is an agricultural waste product that contains high levels of silica. The synthesis of SNPs from RHA offers an environmentally friendly and cost-effective approach to produce SNPs.

Rice husk (RH) accounts for 20% of the total grain weight of rice [5]. It is a byproduct of the rice business that is acquired by default. Because RH landfills are often set on fire, open burning has evolved as the most popular form of RH disposal [6]. Rice growing creates a significant quantity of agro waste, such as straw, husk, and ash, since it is the staple diet for more than 3 billion people, particularly Asians [7,8]. It is expected that more than 120 tons of RH end up as waste material following the milling process each year [9]. Because rice milling is required to create edible rice kernels of high quality, waste management must also conform to

sustainable agriculture and the circular economy [10]. In this research work, we have used Navsari region specific rice's husk named "GNR-3".

Characterization of the synthesized silica nanoparticles was performed using various techniques to assess their suitability for heavy metal remediation. X-ray diffraction (XRD) analysis provided insights into the crystal structure and phase composition of the nanoparticles. Scanning electron microscopy (SEM) and transmission electron microscopy (TEM) allowed for the examination of the morphology, size, and surface characteristics of the nanoparticles. Energy-dispersive X-ray spectroscopy (EDX) was utilized to determine the elemental composition of the nanoparticles. Brunauer-Emmett-Teller (BET) analysis provided information on the specific surface area of the nanoparticles, while atomic force microscopy (AFM) enabled a detailed examination of the nanoparticles' topography.

The primary aim of this study is to develop a sustainable solution for reducing toxic heavy metal contamination in potatoes, specifically the "KUFRI BADASHAH" variety from North Gujarat. To achieve this, we employ mesoporous silica nanoparticles (SNPs) synthesized from rice husk ash (RHA) obtained from the "GNR-3" rice variety in the Navsari region. These SNPs serve as a biomass adsorbent to effectively remove heavy metals, such as Cobalt, Nickel, Lead, and Chromium, from the potato biomass.

In summary, this research aims to enhance food safety and quality by providing a green and cost-effective method for reducing toxic heavy metal levels in potatoes, utilizing readily available agricultural waste materials and minimizing waste generation.

2. Experimental

2.1 Materials

Rice husk (RH) derived from the 'GNR-3 (Gujarat Navsari Rice – 3)' rice variety was sourced from Navsari Agricultural University, Navsari. Potatoes were acquired from the northern Gujarat region known as 'Kufri Badshah'. Analytical reagent-grade hydrochloric acid (HCl) with a concentration of 35-38% was supplied by SDFCL. Deionized water was consistently employed throughout the experiment.

2.2 Methods

2.2.1 Extraction of silica nanoparticles

The first step in the preparation of the rice husk involved a thorough cleaning process to remove any unwanted particles such as dirt, dust, and sand. This cleaning procedure ensured a pristine starting material for further processing. Subsequently, the cleaned rice husk was dried in an oven at a controlled temperature of 100°C for duration of 24 hours, effectively removing any remaining moisture. To modify the rice husk's structure and composition, it underwent a synthesis process with 1 N hydrochloric acid (HCl). This synthesis was conducted at an elevated temperature of 80°C for 2 hours, facilitating the desired chemical changes within the material. After the synthesis step, the acid-treated rice husk was meticulously washed multiple times with distilled water, ensuring the removal of any residual acid and other contaminants. Following the thorough washing process, the acid-treated rice husk was dried once again, this time at a slightly higher temperature of 90°C overnight. This drying stage further prepared the material for the subsequent calcination process. Prior to the crucial calcination step, the dried rice husk was transformed into a powdered form. This powdering process ensured a homogeneous and uniform combustion during calcination. The calcination was carried out in a precisely controlled programmed box furnace, specifically the Lindberg/Blue model, at an elevated temperature of 650°C for duration of 4 hours. This final stage of calcination helped in shaping the rice husk material into its desired form, laying the foundation for its potential applications in various fields (Fig. 1) [11].

Fig. 1: Physical appearance of the different stages of mesoporous nanosilica synthesis

2.2.2 Analytical procedure

In this study, a 200mg of SNPs and varied weights of biomass (400mg, 1000mg and 2000mg) of potato was placed in a conical flask and agitated in a rotary shaker at 250 rpm at room temperature for 6 hours. During our experiments, we determined the weight of biomass to be 400mg, 1000mg and 2000mg. The targeted elements included Co, Ni, Pb, Cr, and Cd - known for their detrimental impact on human health and the environment. To initiate the purification process, the sample was subjected to intense conditions in a microwave digester, precisely the PerkinElmer Titan MPS model, operating at extreme pressure and temperature. This step ensured effective extraction and separation of the targeted metals from the potato samples. For accurate quantification of metal content, the clear filtrate obtained from the extraction process was subjected to analysis using state-of-the-art technology - ICP-MS (Inductively Coupled Plasma Mass Spectrometry). The PerkinElmer NexION 2000 instrument was employed for this purpose, offering exceptional sensitivity and precision in detecting trace metal concentrations. By comparing the metal concentrations at the beginning and end of the process in the aqueous solution, the amount of metal absorbed by the plant biomass was determined. This critical assessment allowed us to understand the effectiveness of the root silica nanoparticle bio-sorbent in the removal of heavy metals from the potatoes, paving the way for sustainable and environmentally responsible agricultural practices in the north Gujarat area [12].

2.2.3 Spectroscopic Analysis

To validate the presence and composition of RH-SNPs, Fourier Transform Infrared (FT-IR) spectroscopy was employed. We utilized the PerkinElmer Spectrum Two, a highly reliable instrument, to meticulously examine the FT-IR spectra of dry RH-SNPs expertly mixed with potassium bromide (KBr). An optimized sample carrier ensured ideal conditions for FT-IR measurements. Spanning the range of 400 to 4000 cm^{-1}, FT-IR analysis comprehensively captured vibrations and interactions within RH-SNPs, providing valuable insights into its molecular composition and structure. This analysis enhances our understanding of RH-SNPs' unique properties and potential applications.

2.2.4 Morphology and Surface Structure

We conducted a detailed examination of RH-SNPs' surface structure and elemental composition using advanced microscopy techniques, including Field Emission Scanning Electron Microscopy (FE-SEM) and Transmission Electron Microscopy (TEM) with Energy Dispersive X-Ray (EDX) capabilities. FE-SEM tests were performed at various magnifications and conditions, with samples coated in gold particles to enhance image clarity. For a comprehensive understanding of shape and diameter formation, TEM examinations utilized a JEOL JEM 2100 instrument with an accelerating voltage of 200 kV. The material was dispersed in a solvent of distilled water and ethanol (2:3) before TEM imaging on copper grids.

2.2.5 Particle Size Analysis and Surface Charge

To investigate RH-SNPs' size distribution and surface charge, we utilized a light scattering device, the HORIBA SZ-100, covering a particle size range of 20 nm to 80 µm. RH-SNPs, dissolved in 0.1% distilled water (DW), were analyzed in an omega cuvette at a back-scattering angle of 170° and a temperature of 25°C. Considering water's refractive index (1.3303) and viscosity (0.8903 mPa), this experiment provided crucial insights into particle size and surface charge characteristics.

2.2.6 Surface Area and Pore Structure Analysis

Material properties were precisely assessed using advanced techniques. Specific surface area and pore size distribution were determined with the Micrometrics ASAP 2010 automated analyzer, employing the Brunauer-Emmett-Teller (BET) technique. Further exploration of microscopic pore size distribution at a molecular level was achieved through indirect molecular adsorption techniques, including nonlocal density functional theory (NLDFT) and N2 isotherms. These analyses unveiled insights into the intricate pore network of the material, providing valuable information for understanding its overall properties.

2.2.7 Surface Topography Analysis

Atomic Force Microscopy (AFM) was employed to conduct a detailed investigation of material surface morphology, offering a comprehensive three-dimensional topographical assessment. Sample was dispersed in deionized water and drop was casted on freshly cleaved mica and dried for 3 hours and then scanned for AFM. The AFM device (VEECO) operated in contact air-mode, capturing high-precision, non-destructive images using nitrite-tipped scanning probes at a frequency of 300 kHz.

2.2.8 Crystallization Structure Analysis

We explored the crystallographic properties of RH-SNPs through X-ray diffraction (XRD) analysis, employing the Smart Lab system from Rigaku, Japan. A radiation of 40 kV and 30 mA illuminated the sample over a two-theta scanning range of 5 to 1000, at a scanning speed of 8.2551° per minute. This meticulous approach yielded precise and detailed XRD spectra, revealing insights into RH-SNPs' crystalline structure and composition. The resulting data plays a crucial role in understanding the unique properties and potential applications of RH-SNPs across diverse scientific and technological fields.

3. Result and discussion

3.1. Characterization of silica nanoparticles (SNPs)

3.1.1. Fourier transforms – infrared analysis (FT-IR)

Figure 2 defines, FT-IR spectrum of the RHA-Silica samples reveals several important bands that correspond to specific functional groups and vibrations. The band at 3457.05 cm^{-1} is attributed to the stretching vibration of the O-H group. This indicates the presence of hydroxyl groups (O-H) in the samples. The band observed at 1649.57 cm^{-1} is common to both silica samples and is attributed to the bending vibration of H_2O molecules in the Si-OH group. This suggests the presence of water molecules associated with the silanol (Si-OH) groups. The bands appearing at 1083.29 cm^{-1} is assigned to the asymmetric stretching vibration of Si-O-Si bonds. This indicates the presence of silicon-oxygen-silicon linkages in the samples. The strong peak observed at 795.48 cm^{-1} is due to the symmetric stretching vibration of Si-O bonds. This suggests the presence of silicon-oxygen (Si-O) bonds in the silica network. The bands at 463.46 cm^{-1} correspond to Si-O bending vibrations of the siloxane groups present in the RHA-Silica samples. This indicates the presence of silicon atoms bonded to oxygen in a bent configuration. The data also indicates that sodium silicate solubilization with hydrochloric acid results in the formation of silanol groups (Si-OH), while siloxane groups are formed through condensation reactions. This information gives insight into the structural changes and functional group transformations that occur during the treatment process (Table. 1).

Table 1: FT-IR spectral data of silica nanoparticles synthesized from GNR-3 rice

Wavenumber (cm^{-1})	Functional Group/ Vibration	Assignment
3457.05	O-H Stretching	Stretching vibration O-H group
1649.57		Bending vibration of H_2O molecule in the Si-OH group
1083.29	Si-O-Si Asymmetric Stretching	Asymmetric stretching vibration of Si-O-Si
795.48	Si-O Symmetric Stretching	Symmetric stretching vibration of Si-O bond
463.46	Si-O Bending (siloxane group)	Si-O bending of siloxane group

Overall, the FT-IR analysis provides valuable information about the composition and bonding characteristics of the RHA-Silica samples, aiding in the understanding of their chemical structure and properties [13-19].

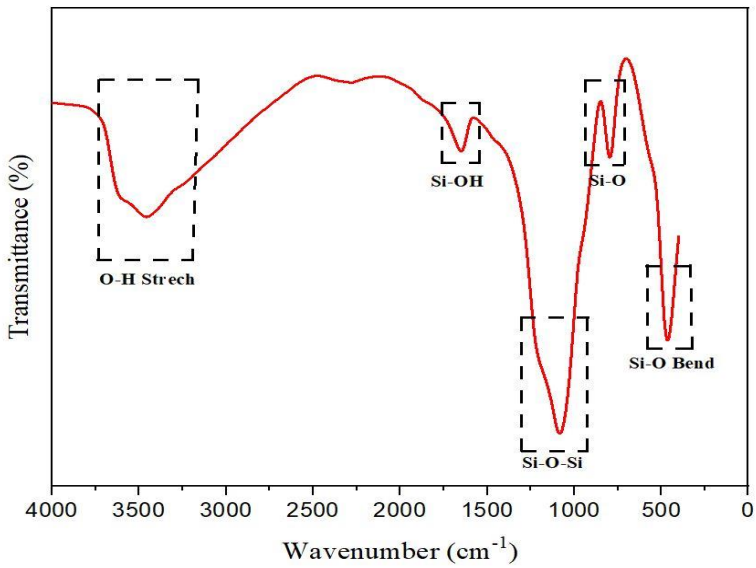

Fig. 2: FT-IR analysis of silica nanoparticles synthesized from GNR-3 rice husk

3.1.2. Scanning electron microscope (SEM)

Figure 4, shows the outcomes of a thorough investigation using scanning electron microscopy (SEM), illuminating the microstructural characteristics of silica nanoparticles made from high-quality rice husk ash (RHA-SNPs). The nanoparticles' size range ranges from 20 to 80 nm. The RHA-SNPs are highly skilled as absorbents for the effective extraction of heavy metal pollutants because to this unique morphological structure, which also endows them with remarkable adsorption properties [20-23].

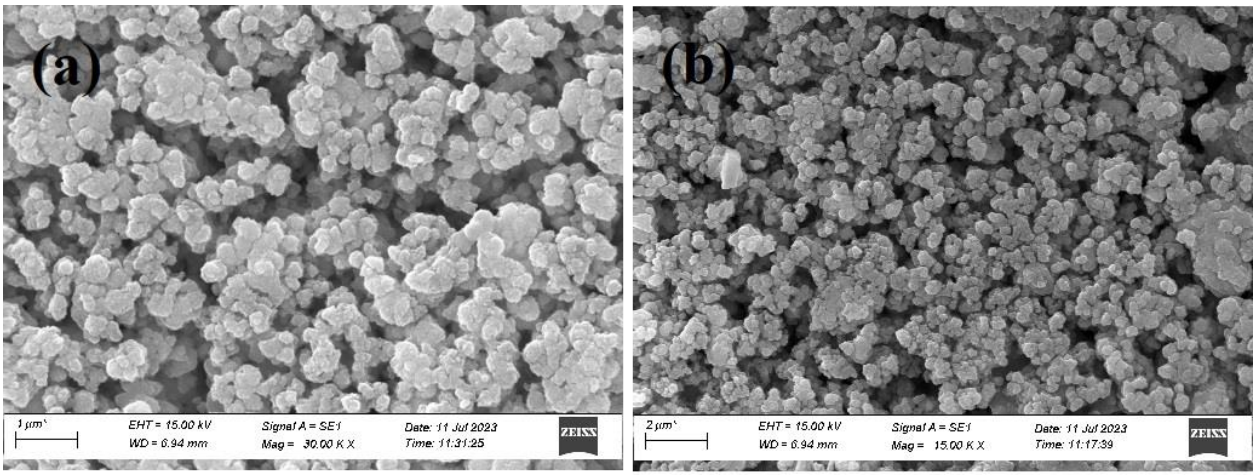

Fig. 3: FE-SEM analysis of silica nanoparticles synthesized from GNR-3 rice husk (a) Scale = 1µm (b) Scale = 2µm

3.1.3. Energy dispersive X-ray analysis (EDX)

The purity of the silica nanoparticles (SNPs) isolated from rice husk (RH) was validated using EDAX analysis. Figure 4; depicts the energy-dispersive X-ray spectroscopy (EDX) spectra of the SNPs. Figure 4(a) displays the SEM picture of the targeted area for EDX investigation. The spectra revealed unique signal peaks for the elements Si (45.36%), O (37.65%), Na (9.84%), and Au (7.14%), as illustrated in Figure 4(b). The EDX spectra confirmed that the produced nanoparticles were silica, since the measured peaks matched those of oxygen and silica. This result indicates the SNP sample's accuracy. Furthermore, the study detected a gold coating, indicating that (Au) was present in the findings [24].

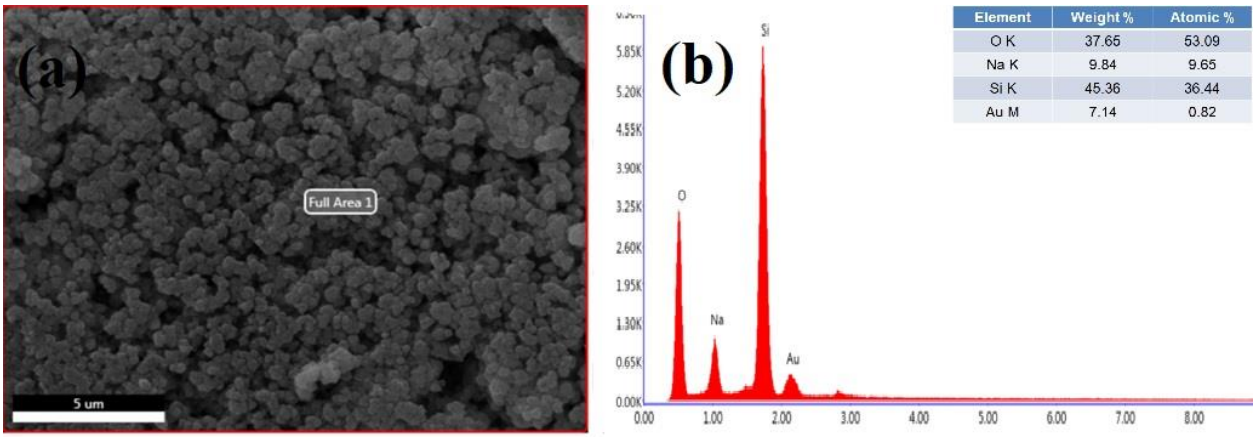

Fig. 4: (a) FE-SEM micrograph (b) EDX spectra of silica nanoparticles synthesized from GNR-3 rice husk

3.1.4. Particle size distribution (PSD)

This study presents a meticulous particle size analysis of high-quality SNPs synthesized from RHA with a dynamic diameter range between 50 and 120 nm, measured using dynamic light scattering (DLS) in water dispersion (Fig. 5). The particle size analyzer reveals a well-dispersed and controlled size distribution, further corroborated by scanning electron microscopy (SEM) analysis. The reason for this is because the DLS technique is often used to estimate the dynamic diameter particle sizes of SNPs distributed in water. The results in the picture further demonstrated that the SiO_2 NPs' particle size distribution is bell-shaped (Gaussian distribution) [25-27].

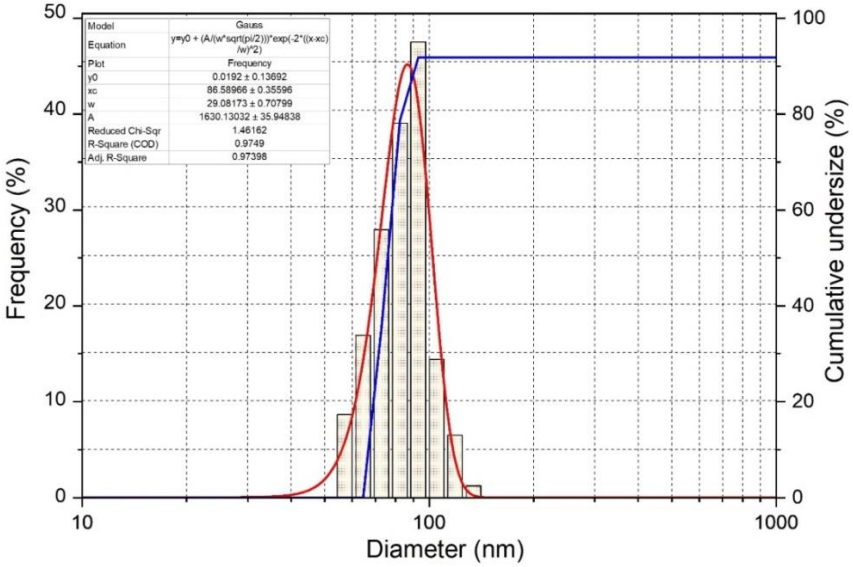

Fig. 5: Particle size analysis of silica nanoparticles synthesized from GNR-3 rice husk

3.1.5. Brunauer-Emmett-Teller (BET)

The BET method, widely acknowledged for its accuracy in determining surface area, was employed to quantify the specific surface area of the silica nanoparticles. The obtained value of 11.1984 m^2/g reflects the extent of surface available for adsorption. Concurrently, the pore size, a crucial factor influencing the accessibility of adsorption sites, was measured at 196.202 Å. The specific surface area of 11.1984 m^2/g suggests a considerable active surface for potential interactions. This parameter is directly correlated with the adsorption capacity of the material, indicating a higher potential for accommodating adsorbate molecules. The synthesis process from rice husk appears to have effectively created a nanoparticle structure conducive to increased surface area. The observed pore size of 196.202 Å is notably large, and such macroscopic pores are known to enhance the accessibility of adsorption sites. Larger pores facilitate the diffusion of adsorbate molecules into the material, contributing to an improved adsorption capability. The synthesis method has evidently resulted in a nanoparticle structure characterized by a significant pore size, which is advantageous for applications requiring efficient adsorption. The combined effect of the substantial specific surface area and larger pore size is anticipated to yield a material with superior adsorption capability. The increased surface area provides more active sites for adsorption, while the larger pores facilitate the swift ingress of adsorbate molecules into the internal structure. This synergistic combination enhances the overall adsorption performance of the silica nanoparticles [28-30].

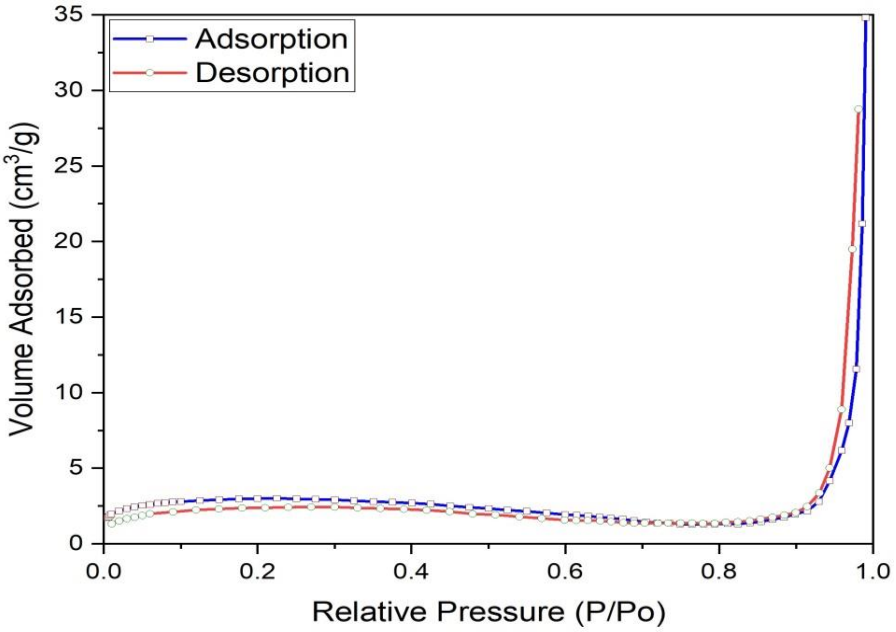

Fig. 6: BET analysis of silica nanoparticles synthesized from GNR-3 rice husk

3.1.6. Transmission electron microscopy (TEM)

Transmission Electron Microscopy (TEM) was employed in this study to thoroughly examine the characteristics of silica nanoparticles (NPs). The analysis encompassed assessments of size, shape, uniformity, and homogeneity, providing valuable insights into the potential applications of these nanoparticles. The size distribution histogram, as depicted in Figure 8(b), was meticulously generated through the utilization of the ImageJ software. This histogram effectively illustrates the frequency distribution of particle sizes. Notably, the histogram exhibits an approximate Log-normal curve, signifying a typical distribution pattern for the silica NPs under investigation. Regarding size and shape, the TEM analysis unveiled that the silica nanoparticles predominantly exhibit spherical morphology. Their diameters were found to span a range of 20 to 50 nm. The most prevalent size within the population was determined to be approximately 33.73 nm. This specific size is indicative of a significant portion of the nanoparticles within the sample, highlighting the reproducibility and consistency of the synthesis process. It's important to note the presence of agglomerates in the TEM images. This phenomenon is attributed to the inherent interactions between smaller particles, primarily driven by electrostatic attraction or Van der Waals forces. Despite being an unavoidable occurrence, these agglomerates don't diminish the overall significance of the findings. In fact, they provide additional information about the interparticle interactions and the forces governing their assembly. Images at different scales are shown in Figure 7 [31-36].

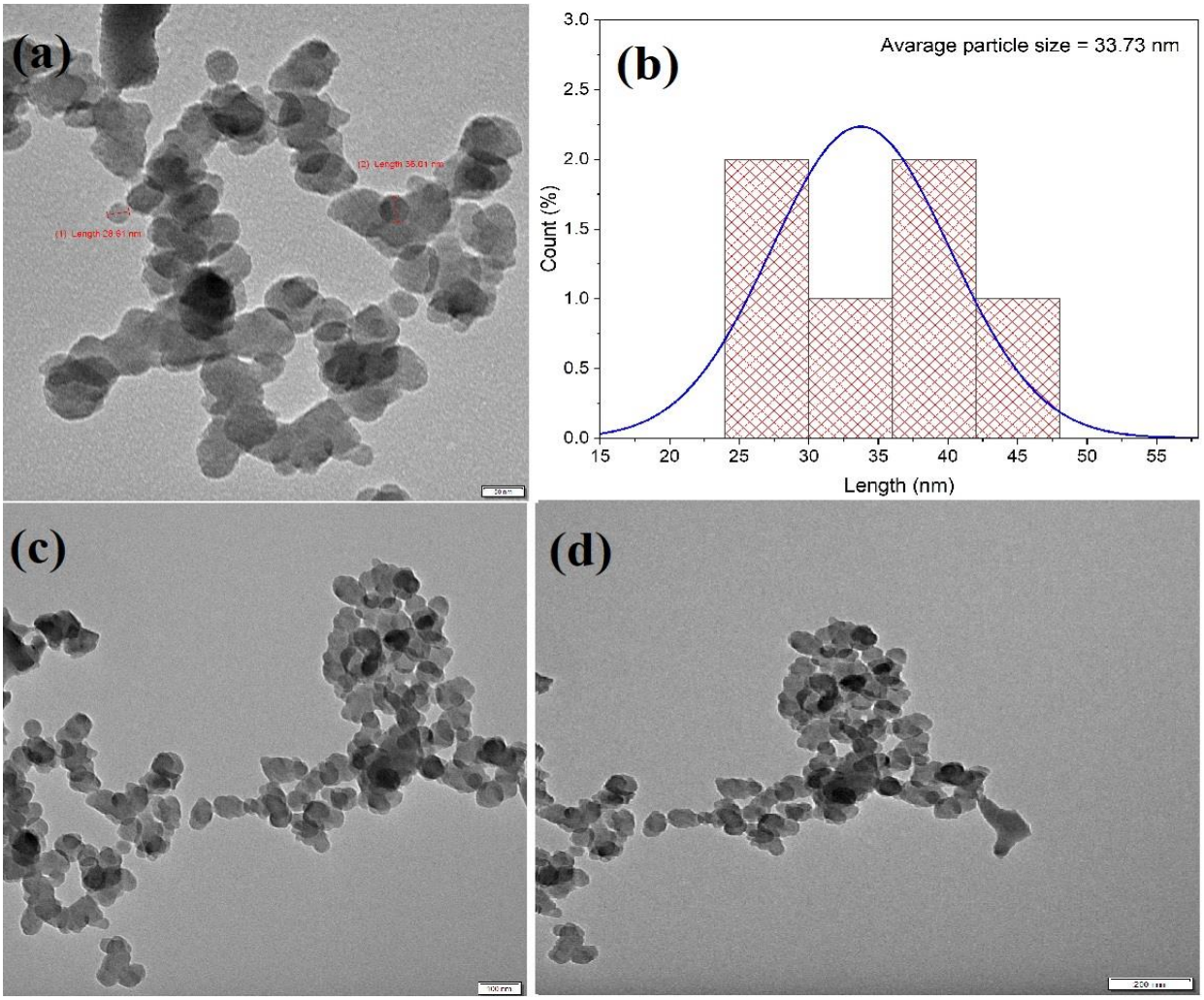

Fig. 7: TEM micrographs of SNPs synthesized from GNR-3 rice husk (a) Scale = 50 nm (b) Graph of average particle size of SNPs (c) Scale = 100 nm (d) Scale = 200 nm

3.1.7. Atomic force microscope (AFM)

The topology of AFM pictures of silica nanoparticles generated from rice husk ash can provide useful insights on the nanoparticles' size, shape, and distribution. The AFM picture will almost certainly show a distribution of silica nanoparticles ranging in size from 20 to 50 nm (Figure 8 (c)). These particles may appear on the surface as small, spherical or semi-spherical structures. Figure 8 (a) (b) (d) shows height

profiles that depict the vertical distance between the tip of the AFM probe and the surface of the material. These profiles will correspond to differences in nanoparticle height throughout the sample. Although there may be some size fluctuation and clustering, you can see how the nanoparticles are distributed around the surface in this image. Figure 8 depicts the surface impurities or pollutants and the underlying structure of the rice husk ash as revealed by AFM images.

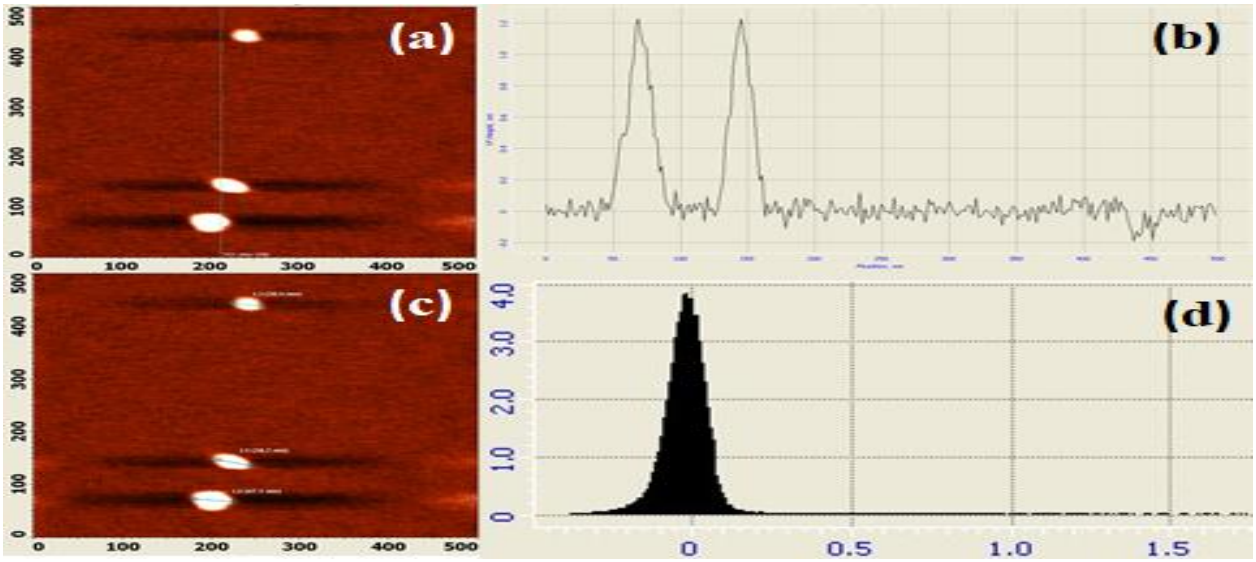

Fig. 8: AFM analysis of SNPs synthesized from GNR-3 rice husk (a) Particle height line (b) Particle height graph (c) Particle size (d) Height histogram

Rice husk ash-based silica nanoparticles might exhibit some degree of surface roughness. This roughness could be due to variations in the synthesis process or the inherent properties of the nanoparticles. Here we might observe clusters or agglomerations of nanoparticles in certain regions of the image. This could indicate a tendency for the nanoparticles to aggregate, which is common in many nanoparticle systems (Figure 9(e-l)). All the images are taken in different micrometers for evaluate and study surface topology and roughness of GNR-3 rice husk ash synthesized SNPs [37-39].

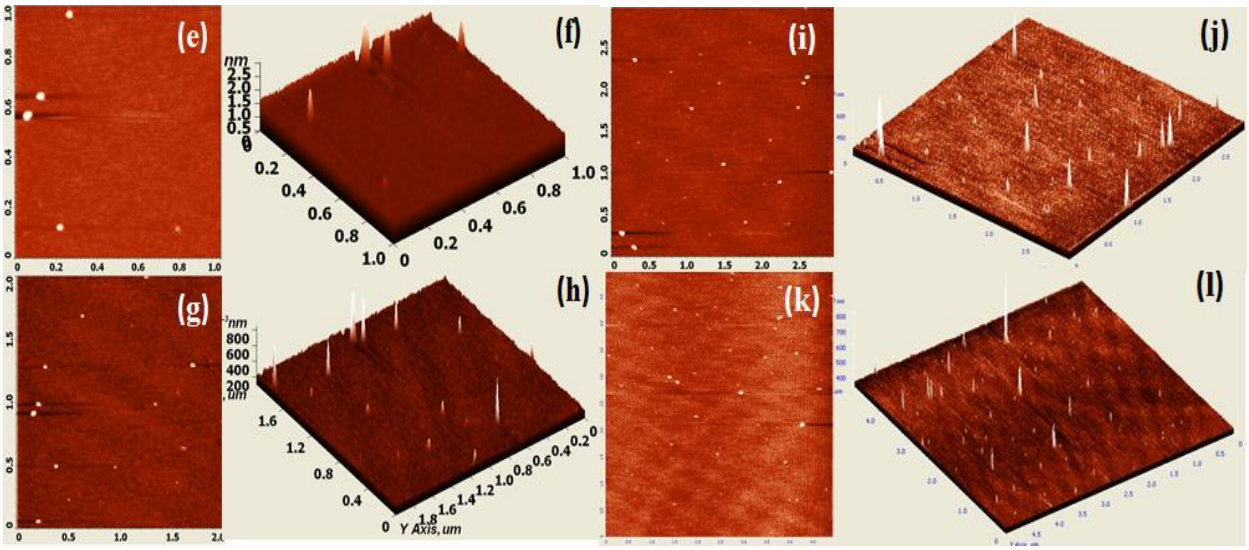

Fig. 9: AFM images of SNPs synthesized from GNR-3 rice husk (e) 1X1µm 2D (f) 1X1µm 3D (g) 2X2µm 2D (h) 2X2µm 3D (i) 3X3µm 2D (j) 3X3µm 3D (k) 5X5µm 2D (l) 5X5µm 3D

3.1.8. X-Ray diffraction (XRD)

The XRD results shown in Figure 10; indicate a wide peak at 2θ between 15° and 35°, and a sharp peak at 2θ = 22.1°, confirming the existence of amorphous SiO_2 and crystalline SiO_2, respectively. RH was thermally treated, resulting in a combination of amorphous and crystalline SiO_2. The strong peak found suggests the creation of tridymite structure, indicating crystalline SiO_2. The intensity peaks at 28.82°, 32.28°, 36.83°, and

46.12° suggest that some of the amorphous phase was changed to crystalline silica structure. The SiO_2 analysis was compared to the silicon oxide SiO_2 powder diffraction file PDF#00-011-0695. The arrows in the diffractograms relate to the primary diffracted peaks. The most notable peak was found at $2\theta = 22.01°$, which corresponded to the (101) plane. For SiO_2, several peaks observed at (111), (102), and (212), while others expanded and were less intense ((101), (200)), indicating that the crystallinity of the silica had decreased. A very wide peak corresponding to the (101) plane was detected, which is typical of a material on the nanometric scale; this broadening might be attributed to scattering induced by nanoparticles. The phase may be classified as amorphous SiO_2 since the amorphous wide peak is placed near the primary peak of the (101) plane of silicon oxide crystalline (Fig. 10) [40-45].

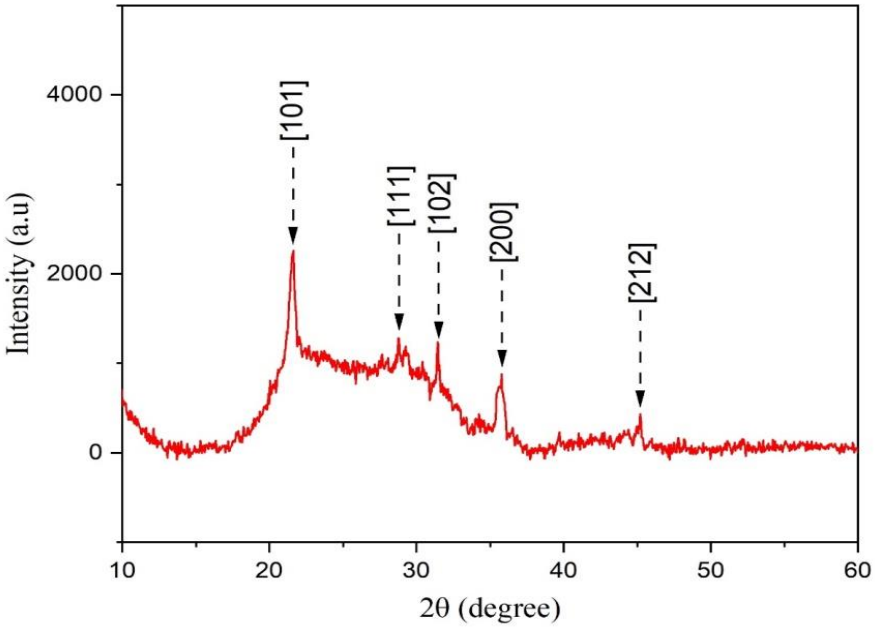

Fig. 10: XRD analysis of silica nanoparticles synthesized from GNR-3 rice husk

3.2. Heavy metal contamination

Heavy metals are a major cause for alarm because they can be both necessary and harmful components of certain organisms. The goal of this research was to examine the concentrations of many metals (Fe, Cu, Zn, Mn, Pb, Ni, and Cd) in sixteen varieties of potatoes grown in Erzurum, Turkey. This study found that the "Kulfi Badshah" named potato cultivars analysed displayed a wide range of variation in the amounts of heavy metals present. Fe > Zn > Mn > Cu > Ni > Pb > Cd is the accumulation order of metals in potato tubers. Food safety is very important, not only for the health of individuals but also for the health of society [46-48]. Some health concerns can be mitigated by eating a variety of foods, but the most significant supply of nutrients still comes from the staples. More than half of the world's population relies on rice as their primary source of nutrition, however the widespread cultivation of rice makes it more susceptible to contamination than other crops. For instance, rice has around a threefold greater tendency to collect heavy metals than wheat [49,50]. There are risks to human health due to heavy metals because of their toxicity, their accumulation in living organisms, and their potential for harmful effects. In an effort to lessen the severity of these health risks, a "maximum allowable concentration," or MAC, of heavy metals in rice has been determined by a consortium of international organisations and national governments. However, even concentrations of heavy metals that are not quite as high as the MAC can be hazardous to human health. According to the findings of several studies, long-term exposure to arsenic at low levels might cause non-carcinogenic disorders such as cancer, hypertension, and neurological issues. In addition, the characteristics that determine exposure shift depending on age, body mass, and location, which increases the risks for populations that are already vulnerable. Because of this, health risk assessments need to take into account, in addition to MAC, other variables such as body weight, age, dietary preferences, and long-term intake (Table 2).[51,52].

Table 2: Effect of SNPs on removal of heavy toxic metals

Replication	Adsorbent dose	Co (%)	Ni (%)	Pb (%)	Cr (%)
R-1	1:2 Potato	1.9568	3.4132	0.8928	3.3378
R-1	1:5 Potato	0.7369	3.6617	0.4367	3.7117
R-1	1:10 Potato	1.2005	3.0718	0.6361	3.8194
R-2	1:2 Potato	1.7529	3.4398	1.4480	3.9646
R-2	1:5 Potato	2.3145	4.5475	1.1471	6.3093
R-2	1:10 Potato	2.0805	4.5591	1.1967	4.6195
R-3	1:2 Potato	4.2609	5.2824	1.3347	9.9880
R-3	1:5 Potato	2.5499	5.7236	1.4992	7.7131
R-3	1:10 Potato	3.4269	5.9233	1.4164	8.4979

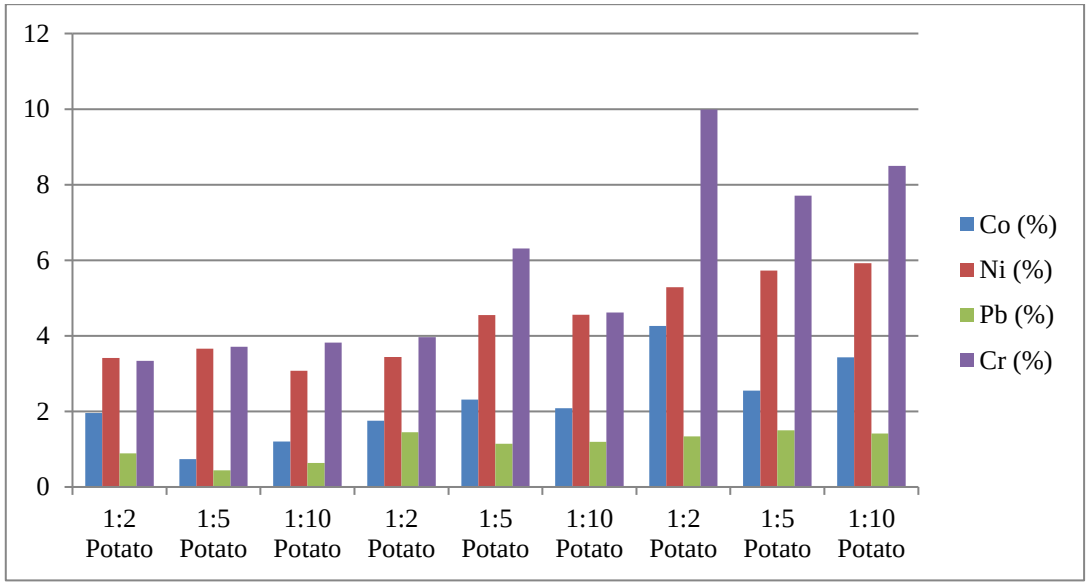

Figure 11: Influence of Synthesized Silica Nanoparticles (SNPs) on the Removal of Toxic Heavy Metals

The data presented in Table 2 offers valuable insights into the impact of Silica Nanoparticles (SNPs) on the removal of harmful heavy metals, including Cobalt (Co), Nickel (Ni), Lead (Pb), and Chromium (Cr), using varying adsorbent doses in multiple replications. A key trend observed is that the effectiveness of SNPs in eliminating these heavy metals is highly dependent on the chosen adsorbent dose. Generally, an increase in the adsorbent dose leads to better removal efficiency, which holds true for all four heavy metals and is consistent across different replications (R-1, R-2, R-3). However, it's important to note that there are specific removal patterns for each heavy metal. For example, Cobalt removal efficiency varies between replications, with different adsorbent doses showing optimal results. Nickel removal is most effective in Replication R-2 at a 1:5 Potato ratio, while in Replication R-3, the 1:10 ratio performs best. Lead removal shows that the 1:2 Potato ratio is consistently less efficient than the 1:5 and 1:10 ratios, while Chromium removal efficiency generally favors the 1:5 and 1:10 Potato ratios. The data also underscores the variability across different replications (R-1, R-2, R-3), which may be attributed to various factors, including experimental conditions and the inherent diversity of heavy metal behavior in different environmental contexts. These findings have practical implications for environmental and health considerations, as they emphasize the importance of carefully selecting the appropriate adsorbent dose based on the target metal and the specific site conditions for effective heavy metal removal (Fig.11).

Further research is essential to refine these findings, determine optimal adsorbent doses for various heavy metals, and account for the variability observed in different replications. This data is a valuable contribution to the field of environmental science, offering guidance for future studies and practical strategies to address heavy metal contamination in environmental and industrial settings.

3.3. Effect of biomass concentration on metal removal

The findings that were analysed and shown in Table 3 indicated that the use of SNPs in the group with ratios of 1:2 (SNPs:Potato), 1:5 (SNPs:Potato), and 1:10 (SNPs:Potato) successfully eliminated harmful heavy metal pollutants that were detected in biomass. Cobalt removal (%) from potatoes using SNPs was found to

be 1.2980.62, 2.0490.28, and 3.4120.87 at the doses 1:2, 1:5, and 1:10 respectively after shaking for 6 hours. Ni = 3.3820.30, 4.1820.64 and 5.6430.33, Pb = 0.6550.22, 1.2640.16 and 1.4170.08, and Cr = 3.6230.25, 4.9641.21 and 8. The ratio of SNPs to potatoes in the 1:10 (SNPs:Potato) and 1:2 (SNPs:Potato) treatments indicated a substantial difference in the elimination of heavy metals. This suggests that the removal of potentially harmful heavy metals from potatoes by SNPs is not affected by the quantity of potatoes present; the process continues regardless. This also suggests that the effectiveness of SNPs in eliminating hazardous heavy metals from potatoes is substantial; even incremental increases in the quantity of potatoes boosted this efficiency.

Table 3: Elimination of high concentrations of heavy hazardous metals

Adsorbent dose	Co (%)	Ni (%)	Pb (%)	Cr (%)
1:2 Potato	1.298±0.62^{b}	3.382±0.30^{b}	0.655±0.22^{b}	3.623±0.25^{b}
1:5 Potato	2.049±0.28^{b}	4.182±0.64^{b}	1.264±0.16^{a}	4.964±1.21^{b}
1:10 Potato	3.412±0.87^{a}	5.643±0.33^{a}	1.417±0.08^{a}	8.733±1.15^{a}
SEm.	0.364	0.260	0.097	0.564
CD	1.259	0.900	0.336	1.952
CV%	27.96	10.23	15.14	16.92

Values are mean±S.D. Treatments with same letters are not significantly different (P<0.05)

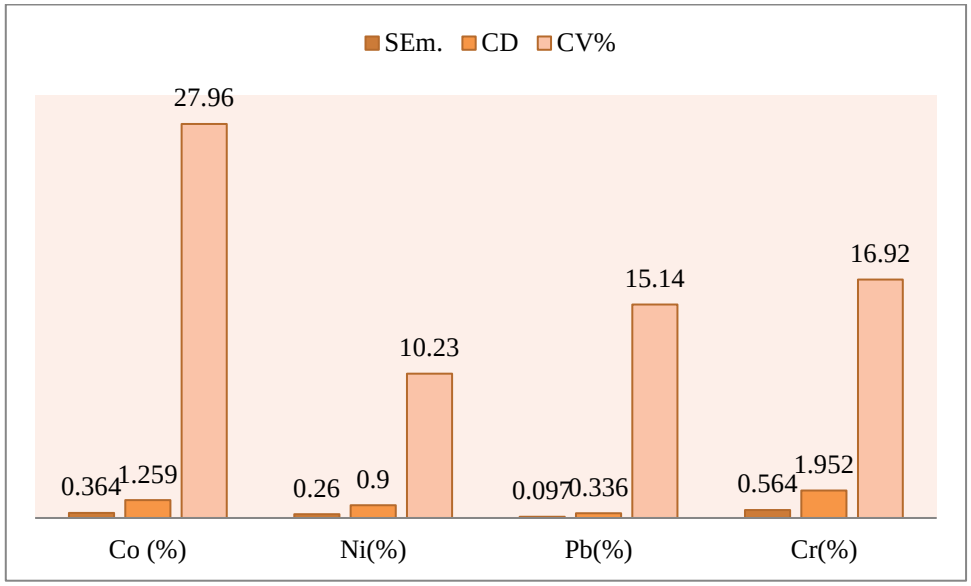

Figure 12: Elimination of high concentrations of heavy hazardous metals

Table 3 presents the results of the study, which focus on the elimination of high concentrations of heavy hazardous metals using various adsorbent doses in the form of Silica Nanoparticles (SNPs) in combination with potatoes. The data offers critical insights into the efficiency of these SNPs in removing specific heavy metals, namely Cobalt (Co), Nickel (Ni), Lead (Pb), and Chromium (Cr). The results are presented in percentages, representing the reduction in metal content after a specified treatment. The table also includes standard error (SEm.), critical difference (CD), and coefficient of variation (CV%) values to provide statistical context for the findings. The outcomes demonstrate a clear trend regarding the effectiveness of the SNPs in eliminating these heavy metals. The table is divided into three columns, each indicating a different adsorbent dose or ratio of SNPs to potatoes. The results are presented for each of the four heavy metals, allowing for a comprehensive assessment of their removal capabilities. In the 1:2 Potato ratio, it is observed that the SNPs were successful in reducing the content of Cobalt by 1.298% with a standard error of 0.62. For Nickel, a reduction of 3.382% was achieved, with a standard error of 0.30. Likewise, Lead saw a reduction of 0.655% with a standard error of 0.22, and Chromium exhibited a reduction of 3.623% with a standard error of 0.25. These results, indicated by the letter "b," signify that there were no statistically significant differences among these values.

When the 1:5 Potato ratio was used, the efficacy of the SNPs in reducing heavy metal content became more apparent. Cobalt displayed a reduction of 2.049% with a standard error of 0.28, while Nickel exhibited a more substantial reduction of 4.182% with a standard error of 0.64. Lead showed a reduction of 1.264% with

a standard error of 0.16, while Chromium underwent a 4.964% reduction with a standard error of 1.21. The notable point here is that for Lead, the value is marked with the letter "a," indicating a statistically significant difference compared to the 1:2 Potato ratio, whereas the other values are not significantly different ("b"). The most remarkable results are observed in the 1:10 Potato ratio, where the SNPs showcased their highest efficiency in heavy metal removal. Cobalt experienced a substantial reduction of 3.412% with a standard error of 0.87, and Nickel displayed an even more impressive reduction of 5.643% with a standard error of 0.33. Lead exhibited a reduction of 1.417% with a standard error of 0.08, and Chromium showed the most substantial reduction of 8.733% with a standard error of 1.15. These results, indicated by the letter "a," signify statistically significant differences compared to both the 1:2 and 1:5 Potato ratios, underscoring the dose-dependent nature of heavy metal removal by SNPs.
The standard error (SEm.) values provide insights into the precision of the measurements, while the critical difference (CD) values help to identify statistically significant differences between treatments. The coefficient of variation (CV%) provides information on the variability of the data (Fig.12).

4. Conclusion

In conclusion, the comprehensive analysis of the data presented in Table 2 reveals reduction of toxic heavy metal contaminants present in North Gujarat region Banaskantha district special variety named “Kufri Badshah” through the strategic utilization of synthesized SNPs derived from Navsari region variety “GNR-3” rice husk. These SNPs were employed at various potato-to-SNP ratios, specifically 1:2, 1:5, and 1:10, demonstrating their notable efficiency in decontaminating biomass, particularly potatoes of the Kufri Badshah variety. Upon subjecting the biomass to a 6-hour interaction with SNPs, we observed significant and dose-dependent reductions in Cobalt, Nickel, Lead, and Chromium concentrations, as highlighted by the respective removal values. For Cobalt, we observed 1.298±0.62, 2.049±0.28, and 3.412±0.87 removal rates at the adsorbent doses of 1:2, 1:5, and 1:10, respectively. Similarly, Nickel exhibited removal rates of 3.382±0.30, 4.182±0.64, and 5.643±0.33, while Lead demonstrated removal rates of 0.655±0.22, 1.264±0.16, and 1.417±0.08 at the same ratios. Chromium removal observed values of 3.623±0.25, 4.964±1.21, and 8.733±1.15, underlining the exceptional potential of SNPs in effectively adsorbing these hazardous heavy metals from potato biomass. A particularly noteworthy observation from this study is the resilience of SNPs even when confronted with increasing potato concentrations. The consistent reduction in toxic heavy metals across different potato-to-SNP ratios suggests that SNPs possess the capability to adsorb and immobilize dangerous toxic heavy metals present in potatoes, irrespective of variations in potato concentrations. This not only highlights the robustness of the SNPs but also implies their significant efficiency in mitigating toxic heavy metal contamination in potato biomass, at least up to higher potato concentrations. These findings hold substantial promise for practical applications in addressing toxic heavy metal contamination issues within agricultural systems and emphasize the potential of rice husk-synthesized SNPs as a viable and sustainable solution for enhancing the safety and quality of agricultural products, such as potatoes, by reducing toxic heavy metal levels. Further research and exploration in this field are warranted to fully harness the potential of SNPs in environmental remediation and agricultural sustainability. Food safety remains a crucial concern for human health, as basic foods form a major part of daily nutrition. Heavy metal contamination poses a significant risk, particularly for staple crops like rice, potato, coffee. The potential for toxic heavy metal accumulation in rice is substantially higher than in other crops, emphasizing the importance of regulating heavy metal concentrations. International organizations and governments have established maximum allowable concentrations (MACs) for specific heavy metals in various foods. This study underscores the cost-efficiency and environmental friendliness of employing SNPs synthesized from rice husk for the removal of toxic heavy metals from food products. By utilizing rice husk waste as the raw material for SNP synthesis, this approach not only effectively removes heavy metals but also minimizes waste generation, as rice husk ash can be repurposed as biomass for further applications in the removal of toxic heavy metals from food products.

References:

1. Manwani, Seema, C. R. Vanisree, Vibha Jaiman, Kumud Kant Awasthi, Chandra Shekhar Yadav, Mahipal Singh Sankhla, Pritam P. Pandit, and Garima Awasthi; "Heavy metal contamination in vegetables and their toxic effects on human health”; Sustainable Crop Production: Recent Advances; 181 (2022).

2. Chen, Yongshan, Jinghua Xu, Zhengyong Lv, Liumei Huang, and Jinping Jiang; "Impacts of biochar and oyster shells waste on the immobilization of arsenic in highly contaminated soils."; Journal of environmental management; 217 (2018) 646-653.
3. Järup, L; "Hazards of heavy metal contamination"; British Medical Bulletin; 68 (2003).
4. İslamoğlu, Ayşe Hümeyra, Tuğba Kahvecioğlu, Gökçe Bönce, Esra Gedik, and Fatma GÜNEŞ. "Determination of heavy metals in some fruits, vegetables and fish by ICP-MS." Eurasian Journal of Food Science and Technology 5, no. 1 (2021): 67-76.
5. Hossain, SK S., Lakshya Mathur, and P. K. Roy. "Rice husk/rice husk ash as an alternative source of silica in ceramics: A review." Journal of Asian Ceramic Societies 6, no. 4 (2018): 299-313.
6. Goodman, Bernard A. "Utilization of waste straw and husks from rice production: A review." Journal of Bioresources and Bioproducts 5, no. 3 (2020): 143-162.
7. FAO, FAOSTAT. "Food and agriculture organization of the United Nations." Rome, URL: http://faostat. fao. org (2018).
8. Moraes, Carlos AM, Iara J. Fernandes, Daiane Calheiro, Amanda G. Kieling, Feliciane A. Brehm, Magali R. Rigon, Jorge A. Berwanger Filho, Ivo AH Schneider, and Eduardo Osorio. "Review of the rice production cycle: by-products and the main applications focusing on rice husk combustion and ash recycling." Waste Management & Research 32, no. 11 (2014): 1034-1048.
9. Bodie, Aaron R., Andrew C. Micciche, Griffiths G. Atungulu, Michael J. Rothrock Jr, and Steven C. Ricke. "Current trends of rice milling byproducts for agricultural applications and alternative food production systems." Frontiers in Sustainable Food Systems 3 (2019): 47.
10. Dhankhar, Poonam, and T. Hissar. "Rice milling." IOSR J. Eng 4, no. 5 (2014): 34-42.
11. Dorairaj, Deivaseeno, Nisha Govender, Sarani Zakaria, and Ratnam Wickneswari. "Green synthesis and characterization of UKMRC-8 rice husk-derived mesoporous silica nanoparticle for agricultural application." Scientific Reports 12, no. 1 (2022): 20162.
12. Sekhar, K. Chandra, C. T. Kamala, N. S. Chary, and Y. Anjaneyulu. "Removal of heavy metals using a plant biomass with reference to environmental control." International Journal of Mineral Processing 68, no. 1-4 (2003): 37-45.
13. Okoronkwo, Elvis A., Patrick Ehi Imoisili, Smart A. Olubayode, and Samuel OO Olusunle. "Development of silica nanoparticle from corn cob ash." Advances in Nanoparticles 5, no. 02 (2016): 135-139.
14. Chen, Jiucun, Mingzhu Liu, Chen Chen, Honghong Gong, and Chunmei Gao. "Synthesis and characterization of silica nanoparticles with well-defined thermoresponsive PNIPAM via a combination of RAFT and click chemistry." ACS applied materials & interfaces 3, no. 8 (2011): 3215-3223.
15. Guo, Wenwen, Guoneng Li, Youqu Zheng, and Ke Li. "Nano-silica extracted from rice husk and its application in acetic acid steam reforming." RSC advances 11, no. 55 (2021): 34915-34922.
16. Nayak, P. P., and A. K. Datta. "Synthesis of SiO2-nanoparticles from rice husk ash and its comparison with commercial amorphous silica through material characterization." Silicon 13, no. 4 (2021): 1209-1214.
17. Vinoda, B. M., M. Vinuth, Y. D. Bodke, and J. Manjanna. "Photocatalytic degradation of toxic methyl red dye using silica nanoparticles synthesized from rice husk ash." J. Environ. Anal. Toxicol 5, no. 1000336 (2015): 2161-0525.
18. Hu, Sixiao, and You-Lo Hsieh. "Preparation of activated carbon and silica particles from rice straw." ACS Sustainable Chemistry & Engineering 2, no. 4 (2014): 726-734.
19. Helmiyati, H., and R. P. Suci. "Nanocomposite of cellulose-ZnO/SiO2 as catalyst biodiesel methyl ester from virgin coconut oil." In AIP conference proceedings, vol. 2168, no. 1. AIP Publishing, 2019.
20. Zhang, Xiaotian, Yangyi Sun, Yijing Mao, Kunlin Chen, Zhihai Cao, and Dongming Qi. "Controllable synthesis of raspberry-like PS–SiO 2 nanocomposite particles via Pickering emulsion polymerization." RSC advances 8, no. 7 (2018): 3910-3918.
21. Alhadhrami, A., Gehad G. Mohamed, Ahmed H. Sadek, Sameh H. Ismail, A. A. Ebnalwaled, and Abdulraheem SA Almalki. "Behavior of silica nanoparticles synthesized from rice husk ash by the sol–gel method as a photocatalytic and antibacterial agent." Materials 15, no. 22 (2022): 8211.
22. Mohseni, Meysam, Kambiz Gilani, and Seyed Alireza Mortazavi. "Preparation and characterization of rifampin loaded mesoporous silica nanoparticles as a potential system for pulmonary drug delivery." Iranian journal of pharmaceutical research: IJPR 14, no. 1 (2015): 27.
23. Zhao, Zongzhe, Chao Wu, Ying Zhao, Yanna Hao, Ying Liu, and Wenming Zhao. "Development of an oral push–pull osmotic pump of fenofibrate-loaded mesoporous silica nanoparticles." International Journal of Nanomedicine (2015): 1691-1701.

24. Abduraimova, Aiganym, Anara Molkenova, Assem Duisembekova, Tomiris Mulikova, Damira Kanayeva, and Timur Sh Atabaev. "Cetyltrimethylammonium bromide (CTAB)-loaded SiO2–Ag mesoporous nanocomposite as an efficient antibacterial agent." Nanomaterials 11, no. 2 (2021): 477.
25. Dang, Nhung Thi Thuy, Trinh Thi Ai Nguyen, Tuan Dinh Phan, Hoa Tran, Phu Van Dang, and Hien Quoc Nguyen. "Synthesis of silica nanoparticles from rice husk ash." VNUHCM Journal of Science and Technology Development 20, no. K7 (2017): 50-54.
26. Saha, Arighna, Kritika Narula, Prashant Mishra, Goutam Biswas, and Snehasis Bhakta. "A facile cost-effective electrolyte-assisted approach and comparative study towards the Greener synthesis of silica nanoparticles." Nanoscale Advances 5, no. 5 (2023): 1386-1396.
27. Patil, Nita Babaso, H. Sharanagouda, S. R. Doddagoudar, C. T. Ramachandra, and K. T. Ramappa. "Biosynthesis and characterization of silica nanoparticles from rice (Oryza sativa L.) husk." Int. J. Curr. Microbiol. App. Sci 7, no. 12 (2018): 2298-2306.
28. Brunauer, S., Emmett, P. H., & Teller, E. (1938). Adsorption of Gases in Multimolecular Layers. Journal of the American Chemical Society, 60(2), 309–319. https://doi.org/10.1021/ja01269a023.
29. Sing, K. S. W. (1985). Reporting Physisorption Data for Gas/Solid Systems with Special Reference to the Determination of Surface Area and Porosity (Recommendations 1984). Pure and Applied Chemistry, 57(4), 603–619. https://doi.org/10.1351/pac198557040603.
30. R. W., Giri, N., & Choudhary, M. (2017). Silica Nanoparticles Synthesis and Applications: A Review. Critical Reviews in Solid State and Materials Sciences, 42(3), 245–277. https://doi.org/10.1080/10408436.2016.1177960.
31. Le, Van Hai, Chi Nhan Ha Thuc, and Huy Ha Thuc. "Synthesis of silica nanoparticles from Vietnamese rice husk by sol–gel method." Nanoscale research letters 8 (2013): 1-10.
32. Rovani, Suzimara, Jonnatan J. Santos, Paola Corio, and Denise A. Fungaro. "Highly pure silica nanoparticles with high adsorption capacity obtained from sugarcane waste ash." ACS omega 3, no. 3 (2018): 2618-2627.
33. Dung, Pham Dinh, Nguyen Ngoc Duy, Nguyen Ngoc Thuy, Lu T. Minh Truc, Bui Van Le, Dang Van Phu, and Nguyen Quoc Hien. "Effect of nanosilica from rice husk on the growth enhancement of chili plant (Capsicum frutescens L.)." Vietnam Journal of Science and Technology 54, no. 5 (2016): 607.
34. Hung, Dao Phi, Nguyen Thien Vuong, Dang Manh Hieu, Nguyen Thi Linh, Trinh Van Thanh, Nguyen Anh Hiep, and Duong Manh Tien. "Effect of silica nanoparticles on properties of coatings based on acrylic emulsion resin." Vietnam Journal of Science and Technology 56, no. 3B (2018): 117-125.
35. AbouAitah, K. E. A., A. A. Farghali, A. Swiderska-Sroda, W. Lojkowski, A. M. Razin, and M. K. Khedr. "Mesoporous silica materials in drug delivery system: pH/glutathione-responsive release of poorly water-soluble pro-drug quercetin from two and three-dimensional pore-structure nanoparticles." J. Nanomed. Nanotechnol 7, no. 02 (2016).
36. Awizar, Denni Asra, Norinsan Kamil Othman, Azman Jalar, Abdul Razak Daud, I. Abdul Rahman, and N. H. Al-Hardan. "Nanosilicate extraction from rice husk ash as green corrosion inhibitor." International Journal of Electrochemical Science 8, no. 2 (2013): 1759-1769.
37. abualnoun Ajeel, Sami, Khalid A. Sukkar, and Naser Korde Zedin. "Extraction of high purity amorphous silica from rice husk by chemical process." In IOP Conference Series: Materials Science and Engineering, vol. 881, no. 1, p. 012096. IOP Publishing, 2020.
38. Kestens, Vikram, Gert Roebben, Jan Herrmann, Åsa Jämting, Victoria Coleman, Caterina Minelli, Charles Clifford et al. "Challenges in the size analysis of a silica nanoparticle mixture as candidate certified reference material." Journal of Nanoparticle Research 18 (2016): 1-22.
39. Moosa, A. Ahmed, and Ban F. Saddam. "Synthesis and characterization of nanosilica from rice husk with applications to polymer composites." American Journal of Materials Science 7, no. 6 (2017): 223-231.
40. Sharma, Sanjeev K., Gaurav Sharma, Abhishek Sharma, Kirti Bhardwaj, Km Preeti, K. Singh, Anirudh Kumar et al. "Synthesis of silica and carbon-based nanomaterials from rice husk ash by ambient fiery and furnace sweltering using a chemical method." Applied Surface Science Advances 8 (2022): 100225.
41. Agi, Augustine, Radzuan Junin, Mohd Zaidi Jaafar, Rahmat Mohsin, Agus Arsad, Afeez Gbadamosi, Cheo Kiew Fung, and Jeffrey Gbonhinbor. "Synthesis and application of rice husk silica nanoparticles for chemical enhanced oil recovery." Journal of Materials Research and Technology 9, no. 6 (2020): 13054-13066.
42. Knipping, Jörg, Hartmut Wiggers, Bernd Rellinghaus, Paul Roth, Denan Konjhodzic, and Cedrik Meier. "Synthesis of high purity silicon nanoparticles in a low pressure microwave reactor." Journal of nanoscience and nanotechnology 4, no. 8 (2004): 1039-1044.

43. F Hincapié Rojas, Daniel, Posidia Pineda Gómez, and Andrés Rosales Rivera. "Production and characterization of silica nanoparticles from rice husk." Advanced Materials Letters 10, no. 1 (2019): 67-73.
44. Atta, A. Y., B. Y. Jibril, B. O. Aderemi, and S. S. Adefila. "Preparation of analcime from local kaolin and rice husk ash." Applied Clay Science 61 (2012): 8-13.
45. Vijayan, R., G. Suresh Kumar, Gopalu Karunakaran, N. Surumbarkuzhali, S. Prabhu, and R. Ramesh. "Microwave combustion synthesis of tin oxide-decorated silica nanostructure using rice husk template for supercapacitor applications." Journal of Materials Science: Materials in Electronics 31 (2020): 5738-5745.
46. Alengebawy, Ahmed, Sara Taha Abdelkhalek, Sundas Rana Qureshi, and Man-Qun Wang. "Heavy metals and pesticides toxicity in agricultural soil and plants: Ecological risks and human health implications." Toxics 9, no. 3 (2021): 42.
47. Tariq, Farah, Xiukang Wang, Muhammad Hamzah Saleem, Zafar Iqbal Khan, Kafeel Ahmad, Ifra Saleem Malik, Mudasra Munir et al. "Risk assessment of heavy metals in basmati rice: Implications for public health." Sustainability 13, no. 15 (2021): 8513.
48. Morgan, Jeffrey N. "Effects of processing on heavy metal content of foods." Impact of processing on food safety (1999): 195-211.
49. Hajeb, P., Jens Jørgen Sloth, S. H. Shakibazadeh, N. A. Mahyudin, and L. Afsah-Hejri. "Toxic elements in food: occurrence, binding, and reduction approaches." Comprehensive Reviews in Food Science and Food Safety 13, no. 4 (2014): 457-472.
50. Hezbullah, M., S. Sultana, S. R. Chakraborty, and M. I. Patwary. "Heavy metal contamination of food in a developing country like Bangladesh: An emerging threat to food safety." Journal of Toxicology and Environmental Health Sciences 8, no. 1 (2016): 1-5.
51. De Toni, Luca, Francesco Tisato, Roberta Seraglia, Marco Roverso, Valentina Gandin, Cristina Marzano, Roberto Padrini, and Carlo Foresta. "Phthalates and heavy metals as endocrine disruptors in food: a study on pre-packed coffee products." Toxicology reports 4 (2017): 234-239.
52. Tajik, Sepideh, Parisa Ziarati, and L. Cruz-Rodriguez. "Coffee waste as novel bio-adsorbent: detoxification of nickel from contaminated soil and Coriandrum Sativum." methods 38, no. 41 (2020): 2693-2504.